Bio-inspired flexible and programmable negative stiffness mechanical metamaterials

Xiaojun Tan, Yifeng Li, Lianchao Wang, Kaili Yao, Qingxiang Ji, Bing Wang*, Vincent Laude, Muamer Kadic**

Xiaojun Tan, Yifeng Li, Lianchao Wang, Kaili Yao, Qingxiang Ji, Bing Wang
National Key Laboratory of Science and Technology on Advanced Composites in Special Environments, Harbin Institute of Technology, Harbin 150080, P.R. China
Email Address: *xiaojun_tan1@163.com, wangbing86@hit.edu.cn, muamer.kadic@gmail.com*

Xiaojun Tan
School of Civil Aviation, Northwestern Polytechnical University, Xi'an 710072, PR China

Xiaojun Tan, Lianchao Wang, Vincent Laude, Muamer Kadic
Institut FEMTO-ST, UMR 6174, CNRS, Université de Bourgogne Franche-Comté, Besançon, France

Yifeng Li
Dept. of Engineering Mechanics, Applied Mechanics Lab., Tsinghua University, Beijing 100084, China

Keywords: *Programmable, Negative Stiffness, Multi-stable, Mechanical Metamaterial, Energy Absorption*

Energy-absorbing materials are widely used under certain high-frequency scenarios, such as cargo packaging or sport protection. Though negative stiffness mechanical metamaterials have many distinctive advantages, fairly low strength and poor specific energy absorption unfortunately limit their present industrial applications. Inspired by the excellent cushioning performance of the paw pads of mammals, a novel flexible energy-absorbing negative stiffness mechanical metamaterial is proposed in this paper. Results show that the presented metamaterial outperforms traditional packaging materials with respect to cushion performance. Moreover, a performance programming strategy is proposed to achieve multistage tuning between large energy absorption and high rebound properties.

1 Introduction

Mechanical metamaterials are man-made by principle and possess distinctive characteristics compared to traditional materials [1–10]. Their properties mainly depend on their architecture rather than on their chemical composition [11–16]. A considerable number of mechanical metamaterial papers have been published during the last two decades. The research objectives of these studies include negative metamaterials (e.g. negative Poisson's ratio [17–21], negative stiffness [22–25], and negative compressibility metamaterials [26–29] etc.), ultra-property metamaterials [30], programmable metamaterials [31–35], and origami-based metamaterials [36,37]. As one of the most often considered topic, negative stiffness mechanical metamaterials (NSMM) show great prospects in various fields, such as elastic wave control [38–46], energy absorption [47–49], advanced actuators [50, 51], and medical implants [52]. When applied to energy absorption, NSMMs possess numerous advantages, including tailorable and high energy absorption efficiency, complete reversibility, as well as a manageable impact response threshold [14]. However, there remain fatal flaws in their properties, i.e. fairly low strength and specific energy absorption [53]. Recently, attention has been paid to solving these issues. Some multi-stable metamaterials can indeed outperform micro-lattices with substantial recoverability [48] and can even approach the performance of rigid foams regarding specific energy absorption [54]. These trials, however, enhance mechanical properties at the expense of the other characteristics of NSMMs. Actually, few typical NSMMs possess a mechanical response similar to commercial energy absorbing materials, such as foams, which implies that NSMMs can hardly be applied in fields such as car crash cushions or aircraft landing buffers, which have serious requirement for specific energy absorption. In the fields of sports and packing, however, the soft and reversible properties

of NSMMs seem quite suitable for the protection of the body of athletes and for the packing of delicate goods [14].

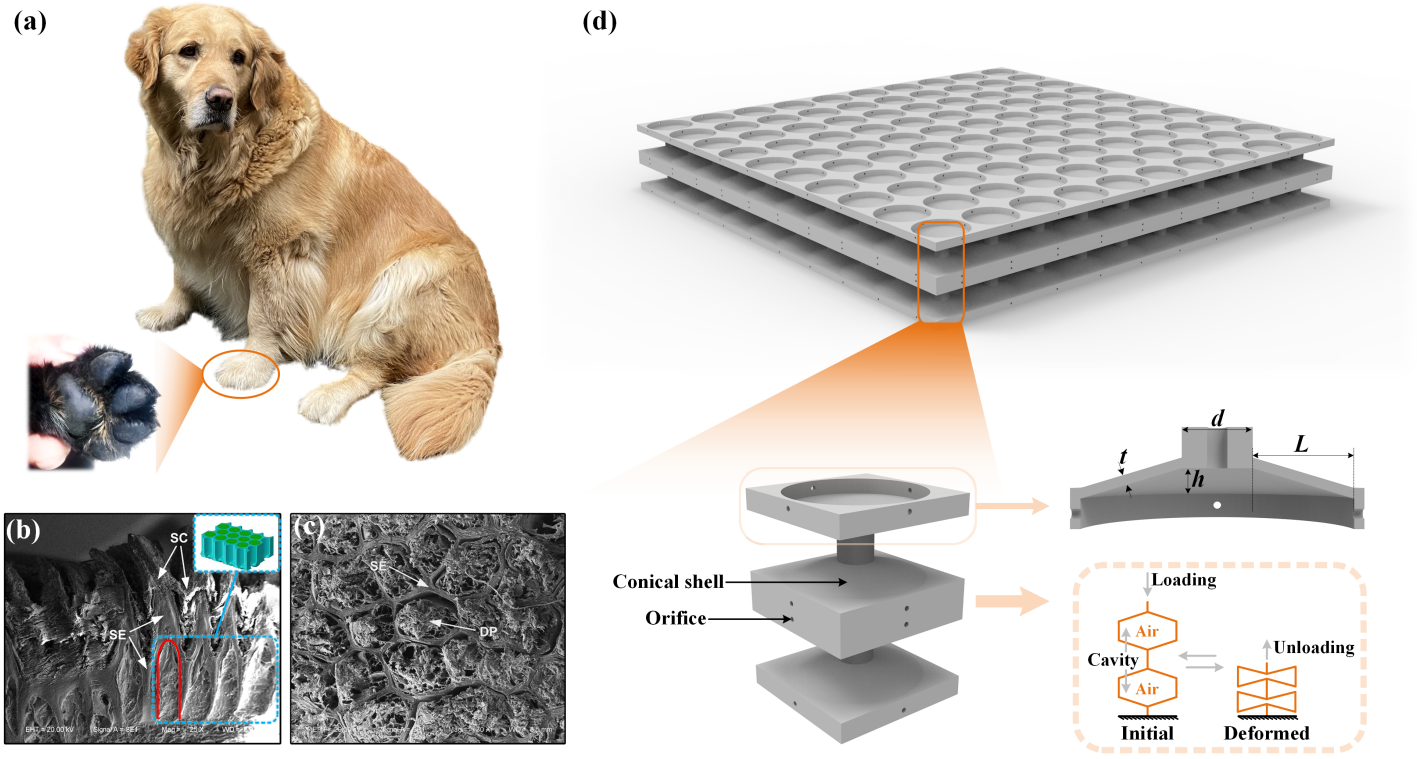

Figure 1: (A) A dog and its paw (image courtesy of Qinghua Wu and Guangbo Liu). (b) Scanning electron microscope images of a dog's stratified epithelium (sagittal section), and it simplified structure [55]. (c) Scanning electron microscope images of a dog's stratified epithelium (transverse section) [55]. (d) Structural diagram of presented negative stiffness mechanical metamaterial, unit cells, and its deformation mode.

Materials for sports protection and packing should adapt well to irregular shapes, in order to wrap the protected objects [56]. Although most NSMMs have low stiffness and strength, the supports used to limit the buckling elements' boundary are rigid, making them hardly foldable and reducing their shape adaptability. In this study, inspired by the internal structure of the pads of mammals (cats and dogs), we design and demonstrate a novel NSMM with improved shape adaptability and programmable energy dissipation properties.

As a result of long-term evolution and natural selection, most mammals have evolved paw pads, and some, such as dogs and cats, possess good ability to run and jump owing to paw pads excellent cushion performance. These paw pads are usually flexible and have a macroscopic convex shape, as illustrated in Fig. 1(a). In addition to the stratum corneum (SC) layer, the convex pad is mainly composed of a stratified epithelium (SE) layer, a dermis layer and a subcutaneous layer. The structure of the SE layer is similar to a honeycomb structure, as observed from the side and section views in Fig. 1(b) and (c) [55]. The combined effect of the dermis and the subcutaneous layers can be regarded as a hydro-static system, or flowable filler. One end of the honeycomb structure is sealed by cone-like shells, as also shown in Fig. 1(b) [55]. The whole pad can be simplified to a periodic structure, as shown in the dotted box. Under the combined effect of the cone-like shells, the honeycomb-like structure and the flowable filler, paw pads exhibit remarkable cushion performance. Inspired by the periodic shell-like structure of the paw pads, we array a conical shell element along three different directions to construct the negative stiffness mechanical metamaterial shown at the top of Fig. 1(d). The close-up view illustrates that two connected shell elements form a cavity and that the enclosed atmosphere enables the tuning of the mechanical response of the solid structure, similar to the combination of dermis and subcutaneous layers. For specific geometric parameters (h, L and t), the

conical shell element exhibits both negative stiffness and bi-stable behavior. Owing to the constraint on the self Hoop stress, these properties are independent of the rigid boundary support. Therefore, the proposed mechanical metamaterial retains almost all advantages of NSMMs while in addition being tunable and easier to fold.

2 Results and discussion

Owing to its structural characteristics, the proposed negative stiffness metamaterial bends and folds more easily than traditional NSMMs, as demonstrated in Fig. 2(a). This characteristics can be useful for the protection of athletes, especially in some high confrontation sports, such as football or basketball, and it can significantly reduce injuries caused by impacts.

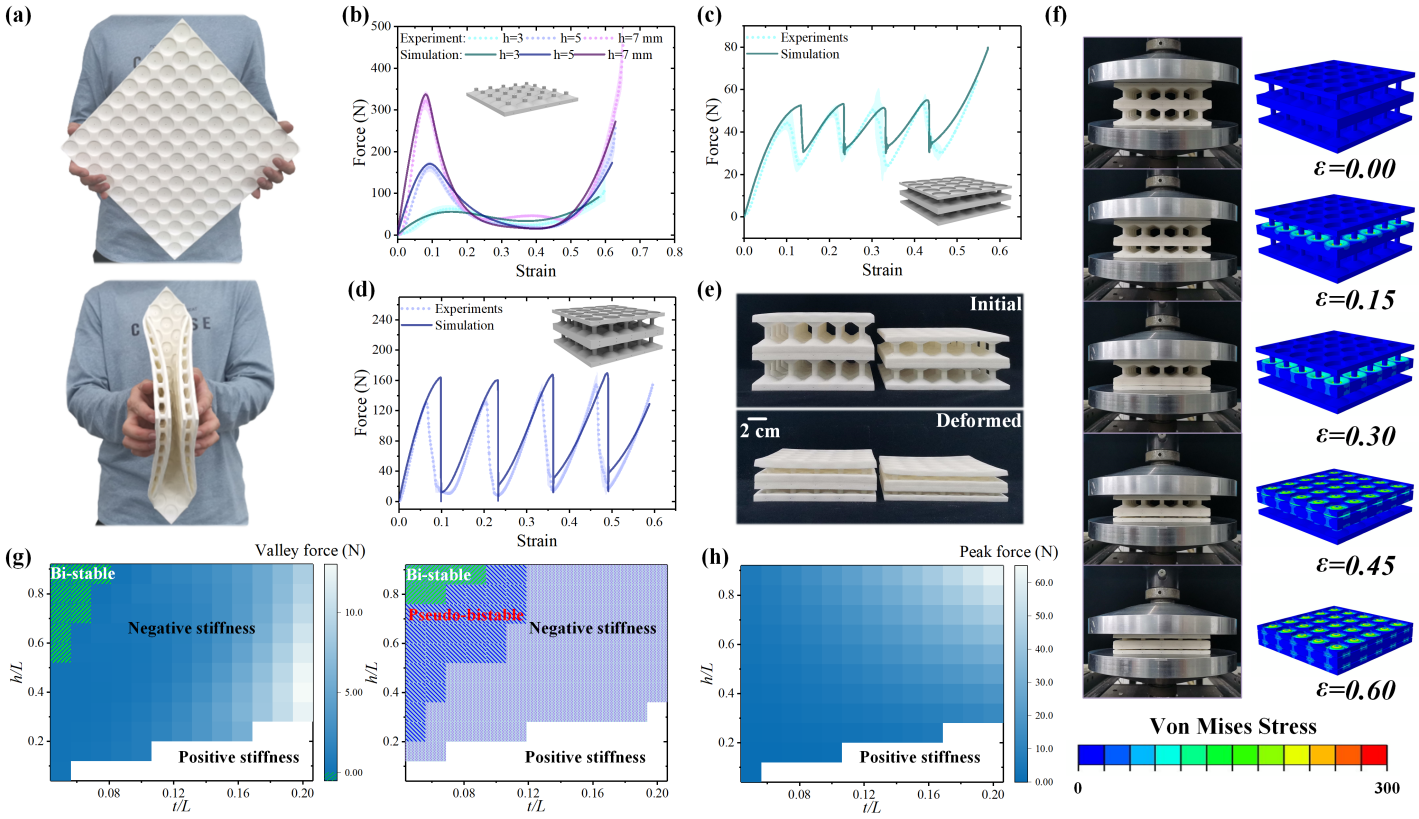

Figure 2: (a) Demonstration of folding of proposed metamaterials. (b) Mechanical response of single layer structure (the colored shadow represents errors in the experiment). Panel (c) and panel (d) present the mechanical response of the negative stiffness mechanical metamaterials with $h = 3$ mm and $h = 5$ mm, respectively. (e) Multi-stable behavior demonstration. (f) Experimental and numerical deformation processes of the metamaterial under compression. (g) Ranges of the structural parameters for different mechanical behaviors, including mono-stable, bistable, and pseudo-bistable: simulation (left) and experiment (right). (h) Relationship between buckling (peak) forces and structure parameters.

The single layer NSMM samples depicted in Fig. 2(a) were additively manufactured and tested. The main structural parameters of the samples are listed in the supplementary file. Their mechanical response, as plotted in Fig. 2(b), features the typical characteristics of traditional negative stiffness elements. Results from experiment and finite element analysis (FEA) primarily reveal the relationship between the arch height h and the response of the unit cell, that is, the stiffness and the strength of the latter increase with the arch height. Moreover, FEA results match well with experimental results. Compression tests were also conducted. Further NSMM samples were constructed by stacking the single layer structures, with the layer number n equaling 4 here. The presented NSMMs (with either $h = 3$ mm or $h = 5$ mm) both show the typical serrated response of traditional NSMMs. The periodic serration, as Fig. 2(c) shows, is dominantly

related to the layer-by-layer gradual collapse of multi-layer NSMMs. The selected video frames in Fig. 2(f) confirm this observation. Regarding both mechanical response and deformation process, simulation results are in good agreement with experimental results for all samples. As illustrated by Fig. 2(e), the presented NSMMs possess a multi-stable behavior for specific structural parameters. Although the force response in Fig. 2(d) does not conform exactly to the response characteristics of multistable metamaterials, i.e., the valley force cannot exceed zero, it still exhibits a pseudo multistable [57] state that is due to the viscoelastic properties of the base material of the structure.

The geometric parameter ranges for positive stiffness, for monostable negative stiffness, for pseudo bistable and bistable behaviors were investigated by FE orthogonal analysis and were further verified by experimental methods. The bistable region and the monostable region are determined from the numerical valley response. However, there always exists a pseudo bistable region in the monostable region. We identify this region through experimental methods. The corresponding results are shown in Fig. 2(g). The parametric boundaries between different response regions are obtained through experiments, as plotted in the right panel. Details of the experiments and of FEA are given in the supplementary file. The critical boundaries obtained from experiments and simulations match well. The critical boundary between the pseudo bistable and the mono-stable negative stiffness regions is also determined. The main difference between both regions is that a pseudo bistable structure will automatically return to its initial state after a certain time, whereas a mono-stable negative stiffness structure recovers immediately. According to the responses associated with different parametric regions, the structural parameters can be selected to satisfy specific requirements. The relationship between structural parameters and peak response was also studied. As shown in Fig. 2(h), the peak force increases with ratios h/L and t/L. The valley value decreases with h/L but increases with t/L.

So far, we have introduced the basic mechanical response characteristics of the proposed materials. Further investigations of their energy absorption and dissipation are conducted in the following. Results are summarized in Fig. 3. The proposed NSMMs are compared with typical traditional energy-absorbing materials, i.e. the air bubble film, air bubble column and the sponge. More details regarding the results of the comparative analysis can be found in the supplementary files. As a whole, the comparison indicates that the proposed NSMMs exhibit better energy absorption and dissipation than the air bubble film and the air bubble column. The specific energy absorption and dissipation of NSMMs further approach and even overcome those of the sponge material. In order to reflect intuitively the performance of energy-absorbing materials, impact experiments were conducted. The basic principle of the impact experiment is to use a gravity driven impact plate to impact the samples and to collect the acceleration response of the impact plate during the whole process, in order to analyze the cushion performance of the samples. The supplementary file gives further details on the impact test. The impact responses of the proposed NSMMs with different structural parameters are shown in the upper panel of Fig. 3(a). The impact responses of the air bubble film and the sponge are shown in the lower panel. The presented acceleration responses have been filtered. Details of the signal processing can be found in the supplementary file. It can be seen from the responses that, like most traditional NSMMs, the acceleration response peak has an obvious response threshold which can be adjusted by the structural parameters. The NSMM with arch height $h = 5$ mm has significantly higher response threshold than that with arch height $h = 3$ mm. For the air bubble films, however thick or thin, the peak value of the acceleration response is almost proportional to the impact height. For the sponge material, the peak acceleration response increases gradually but significantly with impact energy.

The first and the second peaks of the acceleration responses for different structures at different impact height are extracted and compared. The first peak and the second peak are shown in the left and the right sides of Fig. 3(d) respectively. It can be seen that for all structures the first acceleration response peak increases with impact height, i.e. with impact energy. However, the acceleration response for the proposed NSMMs remains almost unchanged as long as the impact height remains smaller than a critical value. Moreover, the impact acceleration response of the NSMM is smaller than that of other traditional

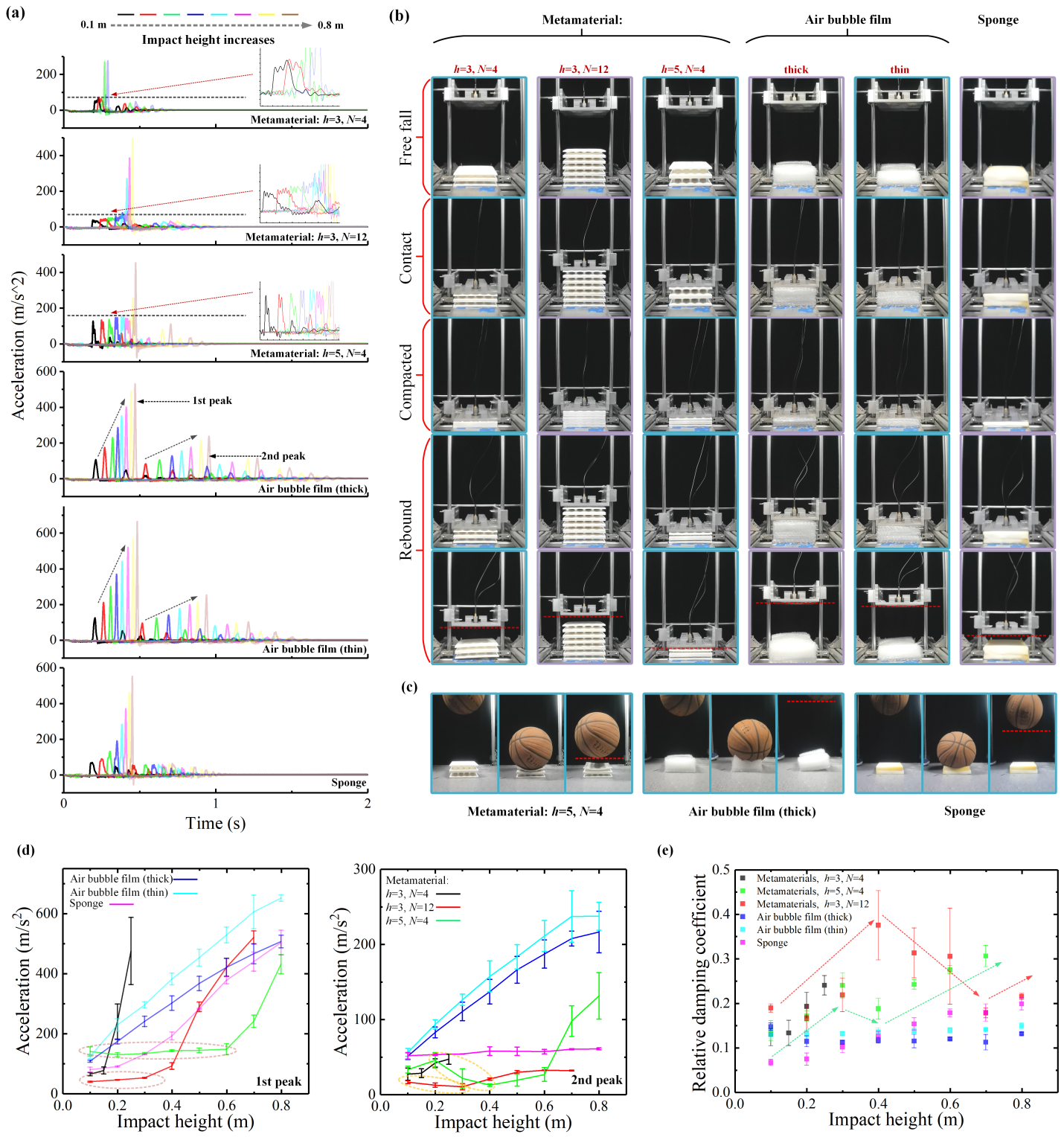

Figure 3: (a) Acceleration response to an impact plate impacting from different heights the proposed metamaterials, the thin and thick air bubble films, and the sponge. (b) Video frames of the impact for the different materials. (c) Demonstration experiment of a basketball released at a height of 1.7 m and impacting different materials, the minimum rebound indicates the best cushion performance. (d) Acceleration response at the first (left side) and the second (right side) impact peaks of response curves in (a). (e) Relative damping coefficient of above materials.

structures. It should be noted that the volumes of these structures are consistent in this analysis, which indicates that the proposed NSMM can achieve better cushion performance when interlocked in the same filling space. The second acceleration peaks of the response are also compared. It can be seen that the difference between the acceleration responses for the air bubble film and the NSMM increases, which indicates that the sponge consumes less energy during the first impact loading and unloading. Therefore, after rebound, the impact plate still has greater impact energy. The second response peak of the sponge remains almost unchanged as the initial impact height increases. This is because the sponge can withstand large structural deformation. In the initial impact loading and unloading process, the mechanical energy consumed by the sponge is directly proportional to the input impact energy, thus the energy of the impact plate changes by a small amount after rebound. The NSMM still has the effect of response suppression on the second response peak, and it is observed that within a certain impact height range the second impact peak even decreases with the initial impact height, as marked by the circle. If the impact energy is too large during the first impact loading, the structure will enter the compact stage after the collapse of the whole structure. The base material of the structure is rubber-like, therefore a large amount of energy is dissipated during the process of extruding the deformed structure, resulting in a great reduction of energy after the first cycle of the impact and further leading to the decrease of the second response peak. From the comparison of the response results for each structure, it can be concluded that the NSMM has significant advantages over the air bubble film and the sponge materials.

As shown in Fig. 3(e), materials are also compared quantitatively with respect to their relative damping coefficient ζ calculated via the equation

$$\ln \eta = \frac{2\pi\zeta}{\sqrt{1-\zeta^2}}, \tag{1}$$

where η is the amplitude reduction factor. More details are given in the supplementary file. As can be observed, the proposed NSMMs possess greater relative damping coefficient no matter how the impact energy changes. The coefficient ζ for the air bubble film remains almost constant. The relative damping coefficient of the sponge increases gradually with the impact energy, because the energy dissipation capacity of the sponge depends significantly on the strain magnitude.

The video frames in Fig. 3(b) illustrate the impact experiments for all considered structures for selected times. The whole response process can be divided into four stages: i) free fall of the impact plate, ii) contact between plate and structure and deformation of the latter, iii) compacting of the structure, and iv) rebound. The bottom part of Fig. 3(b) shows the rebound of the impact plate. It is observed that the rebound of the impact plate is very small on the NSMM, especially in the case $h = 5$ mm for which almost no rebound is observed. This is a direct demonstration of the cushion behavior and the energy absorption performance of the NSMM. The demonstration experiment in Fig. 3(c) vividly illustrates these properties: a basketball freely falls from a height of 1.7 m and impacts either the NSMM, the sponge or the bubble film. The whole process as recorded by a high-speed camera illustrates that the basketball hardly rebounds after impacting the NSMM, whereas it rebounds the highest when impacting the air bubble film. The impact videos for the above tests are provided as supplementary materials.

In addition to the aforementioned characteristics, the proposed NSMM also has another advantage over traditional energy absorbing materials, that is, programmability. Although inspired initially by the paw pads of mamals, the mechanical properties of the proposed NSMM can be programmed by adjusting the internal air pressure. The structure is constructed by arranging truncated conical NS shell elements in a two-dimensional plane and connecting them in series vertically. Through design of a distribution of orifices, air between the units in series can flow freely vertically, whereas it cannot move between units connected in the plane. Therefore, the air pressure between units in series is dynamically balanced and can be set independently of adjacent units. Fig. 4(a) specifically illustrates the programming of alternated high and atmospheric pressure blocks. Of course, the illustration is only for a specific program setting. In addition to the above scheme (referred to as scheme 1), it is equally feasible to remove orifices between cells in

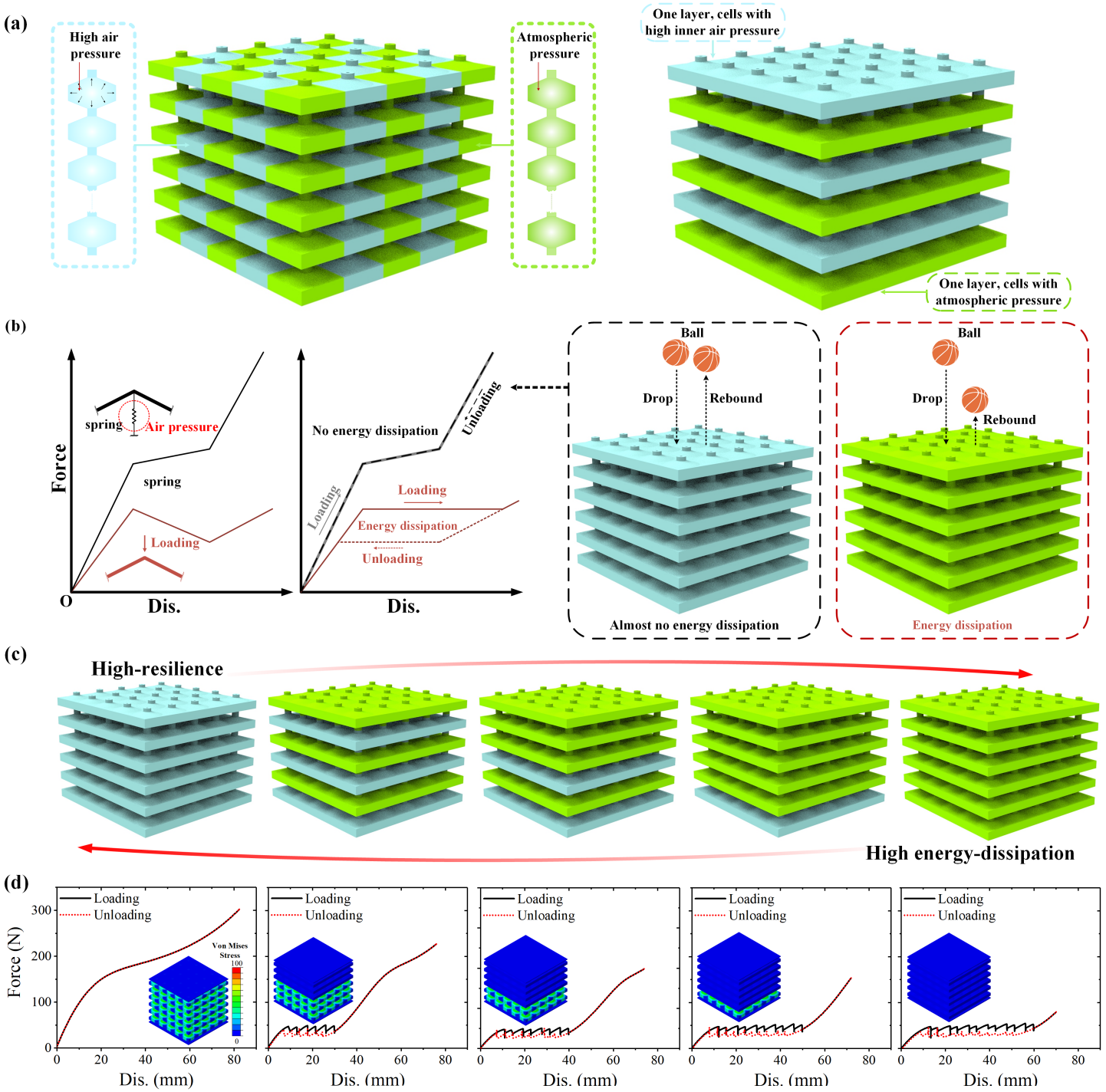

Figure 4: (a) Two programming schemes. In the scheme depicted on the left (scheme 1), air between units in series can flow freely through orifices but cannot move between units connected in the same plane. The internal pressure can be set independently for each set of units, for instance to high or atmospheric pressure. In the scheme depicted on the right (scheme 2), air between units in same plane can flow freely through orifices but not vertically. The internal pressure of each layer is independent. Panel (b) illustrates that the response of negative stiffness elements differs with or without high internal pressure. Under high internal pressure energy dissipation is at a minimum and the rebound is large, whereas under low internal pressure energy dissipation is large and the rebound is minimal. (c) Stacking several metamaterial planes, multi-stage tuning of energy dissipation and rebound is achieved in principle. (d) Proof of such multi-stage tuning through numerical simulations.

series and to add orifices between horizontally connected cells instead (which his referred to as scheme 2). This way, the air pressure in each cell in a given horizontal plane is in dynamical balance and can be programmed using an air pump.

As is well known, when a negative stiffness element is connected in parallel with a spring with large positive stiffness, the combined structure eventually exhibits a positive stiffness. For the NSMM considered in this paper, when the internal air pressure reaches a certain value, the negative stiffness property disappears. When negative stiffness elements with high air pressure are connected in series, the combination is close to the connection of multiple positive stiffness structures in series. In this limit, the snap-through and the snap-back of the structure both disappear, the loading and unloading responses coincide, and there is no energy dissipation during the loading-unloading process, as illustrated by Fig. 4(b). In contrast, in the limit of low internal air pressure, the snap-through and snap-back behaviors result in a hysteretic response with a large envelope area, since the number of cells connected in series increases. Hence, the structure exhibits large energy dissipation. If all parts in series or layers of the structure in Fig. 4(a) have high internal pressure, as shown in the right corner of Fig. 4(b), its energy dissipation capacity is low and an impacting ball would rebound neatly. Conversely, if all parts in series or layers shown in Fig. 4(a) are under atmospheric pressure, the structure can absorb and dissipate energy due to snap-back behavior or multistability. Hence, the rebound of an impacting ball would be much smaller, as also shown in the right corner of the figure, and the structure has good cushioning performance. It is worth noting that the first scheme is not applicable with the proposed NSMM because there is a shear force exerted between the horizontally connected cells and the series structure without snap-back behavior affects the part with snap-back behavior.

The above reasoning suggests using the second scheme to tune the performance of the NSMM. Based on scheme 2, indeed, the structure can be programmed as a high rebound material without energy dissipation, as shown in figure 4(c). Increasing the number of layers under atmospheric pressure, energy dissipation is alternatively improved. The NSMM hence has multi-level adjustable performance and a trade-off between high rebound and high energy absorption can be obtained by digital adjustment. For a structure with n cells in series, and assuming that the number of cells in series that realize snap-back is s, the number of the available states is $n - s$. Energy absorbing materials are widely used in daily life. For example, running shoes with a high rebound midsole can improve running performance but cause great damage to athletes' knees. Running shoes with a high energy absorption midsole can protect athletes well and feel more comfortable, but they do not improve running speed. The programmable NSMM proposed in this paper can be digitally adjusted to trade-off between energy dissipation and rebound, so that the material can be tuned to satisfy practical needs. The programming strategy illustrated in Fig. 4(c) was validated through numerical simulation and the results are plotted in Fig. 4(d). As reflected by the nephogram, layers with high internal pressure show a certain stress in the initial state. The energy dissipation capacity increases gradually as the number of pressurized layers decreases.

3 Conclusion

Inspired by the excellent cushion performance of the paw pads of mamals, a novel NSMM suitable for cargo packaging and sports protection was presented. The static and dynamic mechanical properties were comprehensively investigated and analyzed though a combination of experiments, numerical simulations, and theoretical methods. The results demonstrate that the proposed NSMM not only possesses better energy absorption and dissipation properties than traditional packaging materials, but that it also possesses many of the remarkable characteristics of traditional NSMMs, such as multistability, snap-through, snap-back and so on. Owing to the special architecture of the cell element, the NSMM bends and folds more easily than traditional beam negative stiffness structures, which is conducive to its application in the fields of packaging and sports protection. In addition, taking advantage of the intrinsic sealing property of the structure, a simple scheme was proposed to realize multistage regulation of energy absorption via air pressure programming. This scheme allows multistage switching of the NSMM between high energy

absorption and high rebound. Besides, it can also be a reference for the design of a tunable vibration isolator. Such a mechanism is indeed universal to all NSMMs.

There remain, however, some limitations in this study. Because of the complex architecture of the NSMM, integrated 3D printing technology can not be employed here, resulting in the complex preparation process of this paper. Also limited by the current preparation process and cost, this study does not further explore the role of structural scale in improving material properties. In my opinion, the ideal state of the proposed NSMM in this paper is a kind of material close to the air bubble film, which has many characteristics of negative stiffness metamaterials, meanwhile, is very light mass and requires simple manufacturing process. This goal is promising to be infinitely close in the later stage through topology optimization and parameter analysis.

4 Experimental Section

Design: The key part of the unit cell of the presented NSMM is a truncated conical shell. The bottom of the conical shell is locked in a square frame structure and a cylindrical top part is added for facilitating the formation of the periodic array and the connection of cells. Based on the periodic array of unit cells, the NSMM can be obtained. The cell element can be described by several main parameters, thickness of the shell element, t, height of the shell element, h, outer radius, L, and internal diameter, d. The Orifices shown in Fig. 1(d) can be positioned around the side of each cell element and inside the top column supporting air fluid flow. The setting of the distribution of orifices is very important for the programming of material properties and can be adjusted according to specific requirements.

Sample fabrication: A cavity type structure is hardly fabricated with conventional commercial additive manufacturing technology, such as FDM (Fused Deposition Modeling) or SLS (selective laser sintering). AS a result, the gel-casting method was employed here. The single layer structures were fabricated with the gel-casting method first, before being assembled and glued together. The mold for gel-casting was printed firstly through SLA (Stereo Lithography Apparatus). Injecting the casting urethane elastomer, pre-heated at 50, into the mold, and then demold after 24h at 70 [58, 59]. The base material is Thermoplastic Polyurethane (TPU) whose basic properties were tested according to the ASTM D638-14 standard (more details are given in the supplementary material).

Numerical simulation: In Fig. 2(b-d), the numerical responses are all simulated through the commercial software ABAQUS. Considering that the NSMM is periodic and has a complicated structure, periodic boundary conditions are employed. In Fig. 2(g-h), a large number of numerical calculations have been conducted on different cell elements. Here, Python was applied to build the finite element models of the cell and to run the calculation program. In Fig. 4(d), the influence of the air pressure on the energy dissipation capacity of the NSMM is demonstrated through numerical simulation. Here, the air pressure in the cavity was introduced through the interaction property Fluid cavity in ABAQUS [59].

Properties testing: Quasi-static compression tests, impact tests and some demonstration experiments are conducted to characterize the NSMM's mechanical properties. The Universal testing machine (INSTRON 5569) was employed to implement quasi-static compression. Impact tests and demonstration experiments are realized with the homemade setups (more details can be found in the supplementary material).

Supporting Information
Supporting Information is available from the Wiley Online Library or from the author.

Acknowledgements
This work was supported by China Scholarship Council, the National Natural Science Foundation of China [grant numbers 11972008], the EIPHI Graduate School [grant number ANR-17-EURE-0002] and the French Investissements d'Avenir program, project ISITEBFC [grant number ANR-15-IDEX-03]. This work was supported by the french RENATECH network and its FEMTO-ST technological facility.

References

[1] Corentin Coulais, Dimitrios Sounas, and Andrea Alù. Static non-reciprocity in mechanical metamaterials. *Nature*, 542(7642):461–464, 2017.

[2] Romain Fleury, Dimitrios Sounas, Michael R Haberman, and Andrea Alu. Nonreciprocal acoustics. *Acoustics Today*, 11(3):14–21, 2015.

[3] Amir A Zadpoor. Mechanical meta-materials. *Materials Horizons*, 3(5):371–381, 2016.

[4] Tobias Frenzel, Muamer Kadic, and Martin Wegener. Three-dimensional mechanical metamaterials with a twist. *Science*, 358(6366):1072–1074, 2017.

[5] Huasong Qin, Yingbo Yan, Huichao Liu, Jingran Liu, Yong-Wei Zhang, and Yilun Liu. Modified timoshenko beam model for bending behaviors of layered materials and structures. *Extreme Mechanics Letters*, 39:100799, 2020.

[6] G. W. Milton. *The Theory of Composites*. Cambridge University Press, Cambridge, UK, 2002.

[7] Muamer Kadic, Tiemo Bückmann, Robert Schittny, and Martin Wegener. Experiments on cloaking in optics, thermodynamics and mechanics. *Philosophical Transactions of the Royal Society A: Mathematical, Physical and Engineering Sciences*, 373(2049):20140357, 2015.

[8] Muamer Kadic, Robert Schittny, Tiemo Bückmann, Christian Kern, and Martin Wegener. Hall-effect sign-inversion in a realizable 3d metamaterial. *Physical Review X*, 5:021030, 2015.

[9] Yi Chen, Tobias Frenzel, Sébastien Guenneau, Muamer Kadic, and Martin Wegener. Mapping acoustical activity in 3d chiral mechanical metamaterials onto micropolar continuum elasticity. *Journal of the Mechanics and Physics of Solids*, 137:103877, 2020.

[10] Xiaojun Tan, Julio Andrés Iglesias Martínez, Gwenn Ulliac, Bing Wang, Linzhi Wu, Johnny Moughames, Marina Raschetti, Vincent Laude, and Muamer Kadic. Single-step-lithography microstepper based on frictional contact and chiral metamaterial. *Small*, 18(28):2202128, 2022.

[11] Aleksi Bossart, David MJ Dykstra, Jop van der Laan, and Corentin Coulais. Oligomodal metamaterials with multifunctional mechanics. *Proceedings of the National Academy of Sciences*, 118(21), 2021.

[12] Bastiaan Florijn, Corentin Coulais, and Martin van Hecke. Programmable mechanical metamaterials: the role of geometry. *Soft Matter*, 12(42):8736–8743, 2016.

[13] Ahmad Rafsanjani, Abdolhamid Akbarzadeh, and Damiano Pasini. Snapping mechanical metamaterials under tension. *Advanced Materials*, 27(39):5931–5935, 2015.

[14] Sicong Shan, Sung H Kang, Jordan R Raney, Pai Wang, Lichen Fang, Francisco Candido, Jennifer A Lewis, and Katia Bertoldi. Multistable architected materials for trapping elastic strain energy. *Advanced Materials*, 27(29):4296–4301, 2015.

[15] M. Kadic, G. M. Milton, M. van Hecke, and M. Wegener. 3d metamaterials. *Nature Reviews Physics*, 1,:198–210, 2019.

[16] G. W. Milton. Complete characterization of the macroscopic deformations of periodic unimode metamaterials of rigid bars and pivots. *Journal of the Mechanics and Physics of Solids*, 61,:1543–1560, 2013.

[17] Helena MA Kolken, Shahram Janbaz, Sander MA Leeflang, Karel Lietaert, Harrie H Weinans, and Amir A Zadpoor. Rationally designed meta-implants: a combination of auxetic and conventional meta-biomaterials. *Materials Horizons*, 5(1):28–35, 2018.

[18] T. A. M. Hewage, K. L. Alderson, A. Alderson, and F. Scarpa. Double-negative mechanical metamaterials displaying simultaneous negative stiffness and negative poissons ratio properties. *Advanced Materials*, 28,:10323–10332, 2016.

[19] K. E. Evans and A. Alderson. Auxetic materials: Functional materials and structures from lateral thinking! *Advanced Materials*, 12,:617–628, 2000.

[20] Krzysztof K Dudek, Julio A Iglesias Martínez, Gwenn Ulliac, and Muamer Kadic. Micro-scale auxetic hierarchical mechanical metamaterials for shape morphing. *Advanced Materials*, 34(14):2110115, 2022.

[21] Joseph N Grima, Rosie Jackson, Andrew Alderson, and Kenneth E Evans. Do zeolites have negative poisson's ratios? *Advanced Materials*, 12(24):1912–1918, 2000.

[22] Tobias Frenzel, Claudio Findeisen, Muamer Kadic, Peter Gumbsch, and Martin Wegener. Tailored buckling microlattices as reusable light-weight shock absorbers. *Advanced Materials*, 28(28):5865–5870, 2016.

[23] Fei Pan, Yilun Li, Zhaoyu Li, Jialing Yang, Bin Liu, and Yuli Chen. 3d pixel mechanical metamaterials. *Advanced Materials*, 31(25):1900548, 2019.

[24] Yizhe Liu, Fei Pan, Bin Ding, Yilong Zhu, Kuijian Yang, and Yuli Chen. Multistable shape-reconfigurable metawire in 3d space. *Extreme Mechanics Letters*, 50:101535, 2022.

[25] Huasong Qin, Yu Sun, Jefferson Zhe Liu, Mengjie Li, and Yilun Liu. Negative poisson's ratio in rippled graphene. *Nanoscale*, 9(12):4135–4142, 2017.

[26] Jingyuan Qu, Alexander Gerber, Frederik Mayer, Muamer Kadic, and Martin Wegener. Experiments on metamaterials with negative effective static compressibility. *Physical Review X*, 7(4):041060, 2017.

[27] K. K. Dudek, D. Attard, R. Caruana-Gauci, K. W. Wojciechowski, and J. N. Grima. Unimode metamaterials exhibiting negative linear compressibility and negative thermal expansion. *Smart Mater. Struct.*, 25,:025009, 2016.

[28] Jingyuan Qu, Muamer Kadic, and Martin Wegener. Three-dimensional poroelastic metamaterials with extremely negative or positive effective static volume compressibility. *Extreme Mechanics Letters*, 22:165–171, 2018.

[29] Xin Lin, Fei Pan, Kang Yang, Juan Guan, Bin Ding, Yizhe Liu, Kuijian Yang, Bin Liu, and Yuli Chen. A stair-building strategy for tailoring mechanical behavior of re-customizable metamaterials. *Advanced Functional Materials*, 31(37):2101808, 2021.

[30] Xiaoyu Zheng, Howon Lee, Todd H Weisgraber, Maxim Shusteff, Joshua DeOtte, Eric B Duoss, Joshua D Kuntz, Monika M Biener, Qi Ge, Julie A Jackson, et al. Ultralight, ultrastiff mechanical metamaterials. *Science*, 344(6190):1373–1377, 2014.

[31] Corentin Coulais, Eial Teomy, Koen De Reus, Yair Shokef, and Martin Van Hecke. Combinatorial design of textured mechanical metamaterials. *Nature*, 535(7613):529–532, 2016.

[32] Bastiaan Florijn, Corentin Coulais, and Martin van Hecke. Programmable mechanical metamaterials. *Physical Review Letters*, 113(17):175503, 2014.

[33] F. Wenz, I. Schmidt, A. Leichner, T. Lichti, S. Baumann, H. Andrae, and C. Eberl. Designing shape morphing behavior through local programming of mechanical metamaterials. *Advanced Materials*, 33,:2008617, 2021.

[34] Xuan Zhang, Qi Wang, Ruiping Zou, Bo Song, Chunze Yan, Yusheng Shi, and Bin Su. 3d-printed superhydrophobic and magnetic device that can self-powered sense a tiny droplet impact. *Engineering*, 2022.

[35] Zheng Ma, Qi Wang, Zhenhua Wu, Dezhi Chen, Chunze Yan, Yusheng Shi, Michael D Dickey, and Bin Su. A superconducting-material-based maglev generator used for outer-space. *Advanced Materials*, 34(33):2203814, 2022.

[36] Jesse L Silverberg, Arthur A Evans, Lauren McLeod, Ryan C Hayward, Thomas Hull, Christian D Santangelo, and Itai Cohen. Using origami design principles to fold reprogrammable mechanical metamaterials. *Science*, 345(6197):647–650, 2014.

[37] C. Coulais, A. Sabbadini, F. Vink, and M. van Hecke. Multi-step self-guided pathways for shape-changing metamaterials. *Nature*, 561,:512–515, 2018.

[38] R. Fleury, D. L. Sounas, and A. Alú. An invisible acoustic sensor based on parity-time symmetry. *Nature Communications*, 6,:5905, 2015.

[39] Lishuai Jin, Romik Khajehtourian, Jochen Mueller, Ahmad Rafsanjani, Vincent Tournat, Katia Bertoldi, and Dennis M Kochmann. Guided transition waves in multistable mechanical metamaterials. *Proceedings of the National Academy of Sciences*, 117(5):2319–2325, 2020.

[40] R. Fleury, D. L. Sounas, C. F. Fleck, M. R. Haberman, and A. Alú. Sound isolation and giant linear nonreciprocity in a compact acoustic circulator. *Science*, 343,:516–519, 2014.

[41] Yi Chen, Muamer Kadic, Sébastien Guenneau, and Martin Wegener. Isotropic chiral acoustic phonons in 3d quasicrystalline metamaterials. *Physical Review Letters*, 124(23):235502, 2020.

[42] Yi Chen, Muamer Kadic, and Martin Wegener. Chiral triclinic metamaterial crystals supporting isotropic acoustical activity and isotropic chiral phonons. *Proceedings of the Royal Society A*, 477(2246):20200764, 2021.

[43] Yi Chen, Muamer Kadic, and Martin Wegener. Roton-like acoustical dispersion relations in 3d metamaterials. *Nature communications*, 12(1):1–8, 2021.

[44] Julio Andrés Iglesias Martínez, Michael Fidelis Groß, Yi Chen, Tobias Frenzel, Vincent Laude, Muamer Kadic, and Martin Wegener. Experimental observation of roton-like dispersion relations in metamaterials. *Science Advances*, 7(49):eabm2189, 2021.

[45] Ke Wang, Yi Chen, Muamer Kadic, Changguo Wang, and Martin Wegener. Nonlocal interaction engineering of 2d roton-like dispersion relations in acoustic and mechanical metamaterials. *Communications Materials*, 3(1):1–11, 2022.

[46] Julio Andrés Iglesias Martínez, Nicolas Laforge, Muamer Kadic, and Vincent Laude. Topological waves guided by a glide-reflection symmetric crystal interface. *Physical Review B*, 106(6):064304, 2022.

[47] B. Florijn, C. Coulais, and M. van Hecke. Programmable mechanical metamaterials. *Physical Review Letters*, 113,:175503, 2014.

[48] Babak Haghpanah, Ladan Salari-Sharif, Peyman Pourrajab, Jonathan Hopkins, and Lorenzo Valdevit. Multistable shape-reconfigurable architected materials. *Advanced Materials*, 28(36):7915–7920, 2016.

[49] Peng Chen, Haoze Wang, Jin Su, Yujia Tian, Shifeng Wen, Bin Su, Cao Yang, Binling Chen, Kun Zhou, Chunze Yan, et al. Recent advances on high-performance polyaryletherketone materials for additive manufacturing. *Advanced Materials*, 34(52):2270360, 2022.

[50] Yichao Tang, Yinding Chi, Jiefeng Sun, Tzu-Hao Huang, Omid H Maghsoudi, Andrew Spence, Jianguo Zhao, Hao Su, and Jie Yin. Leveraging elastic instabilities for amplified performance: Spine-inspired high-speed and high-force soft robots. *Science Advances*, 6(19):eaaz6912, 2020.

[51] Qi Wang, Zhenhua Wu, Jianyu Huang, Zhuolin Du, Yamei Yue, Dezhi Chen, Dong Li, and Bin Su. Integration of sensing and shape-deforming capabilities for a bioinspired soft robot. *Composites Part B: Engineering*, 223:109116, 2021.

[52] FSL Bobbert, Shahram Janbaz, T van Manen, Yageng Li, and AA Zadpoor. Russian doll deployable meta-implants: Fusion of kirigami, origami, and multi-stability. *Materials & Design*, 191:108624, 2020.

[53] Katia Bertoldi. Harnessing instabilities to design tunable architected cellular materials. *Annual Review of Materials Research*, 47:51–61, 2017.

[54] Shaowei Zhu, Xiaojun Tan, Bing Wang, Shuai Chen, Jiqiang Hu, Li Ma, and Linzhi Wu. Bio-inspired multistable metamaterials with reusable large deformation and ultra-high mechanical performance. *Extreme Mechanics Letters*, 32:100548, 2019.

[55] Huaibin Miao, Jun Fu, Zhihui Qian, Luquan Ren, and Lei Ren. How does the canine paw pad attenuate ground impacts? a multi-layer cushion system. *Biology open*, 6(12):1889–1896, 2017.

[56] Lishuai Jin, Antonio Elia Forte, Bolei Deng, Ahmad Rafsanjani, and Katia Bertoldi. Kirigami-inspired inflatables with programmable shapes. *Advanced Materials*, 32(33):2001863, 2020.

[57] A Brinkmeyer, M Santer, A Pirrera, and PM Weaver. Pseudo-bistable self-actuated domes for morphing applications. *International Journal of Solids and Structures*, 49(9):1077–1087, 2012.

[58] Bing Wang, Xiaojun Tan, Shaowei Zhu, Shuai Chen, Kaili Yao, Peifei Xu, Lianchao Wang, Huaping Wu, and Yuguo Sun. Cushion performance of cylindrical negative stiffness structures: Analysis and optimization. *Composite Structures*, 227:111276, 2019.

[59] Xiaojun Tan, Shuai Chen, Bing Wang, Jie Tang, Lianchao Wang, Shaowei Zhu, Kaili Yao, and Peifei Xu. Real-time tunable negative stiffness mechanical metamaterial. *Extreme Mechanics Letters*, 41:100990, 2020.